remote sensing

Article

Evaluation of Spatial and Temporal Variations in the Difference between Soil and Air Temperatures on the Qinghai–Tibetan Plateau Using Reanalysis Data Products

Xiqiang Wang and Rensheng Chen *

Qilian Alpine Ecology and Hydrology Research Station, Key Laboratory of Ecological Safety and Sustainable Development in Arid Lands, Northwest Institute of Eco-Environment and Resources, Chinese Academy of Sciences, Lanzhou 730000, China; wangxq@lzb.ac.cn
* Correspondence: crs2008@lzb.ac.cn

Abstract: Many extreme meteorological events are closely related to the strength of land–atmosphere interactions. In this study, the heat exchange regime between the shallow soil layer and the atmosphere over the Qinghai–Tibetan Plateau (QTP) was investigated using a reanalysis dataset. The analysis was conducted using a simple metric ΔT, defined as the difference between the temperatures of the shallow soil and the air. First, the performance of 4 widely used reanalysis data products (GLDAS-Noah, NCEP-R2, ERA5 and ERA5-land) in estimating ΔT on the QTP at soil depths of 0~7 or 0~10 cm was evaluated during the baseline period (1981–2010); the ERA5-land product was selected for subsequent analysis, because it yielded a better performance in estimating the annual and seasonal ΔT and finer spatial resolution than the other datasets. Using the soil temperature at depths of 0~7 cm and the air temperature at 2 m above the ground, as provided by the ERA5-Land reanalysis dataset, the entire QTP was found to be dominated by a positive ΔT both annually and seasonally during the baseline period, with large differences in the spatial distribution of the seasonal values of ΔT. From 1950 to 2021, the QTP experienced a significant decreasing trend in the annual ΔT at a rate of -0.07 °C/decade, and obvious decreases have also been detected at the seasonal level (except in spring). In the southern and northeastern parts of the QTP, rapid rates of decrease in the annual ΔT were detected, and the areas with significantly decreasing trends in ΔT were found to increase in size gradually from summer, through autumn, to winter. This study provides a holistic view of the spatiotemporal variations in ΔT on the QTP, and the findings can improve our understanding of the land–atmosphere thermal interactions in this region and provide important information pertaining to regional ecological diversity, hydrology, agricultural activity and infrastructural stability.

Keywords: land–atmosphere interaction; soil temperature; air temperature; ERA5-land; Qinghai–Tibetan Plateau

check for updates

Citation: Wang, X.; Chen, R. Evaluation of Spatial and Temporal Variations in the Difference between Soil and Air Temperatures on the Qinghai–Tibetan Plateau Using Reanalysis Data Products. *Remote Sens.* **2023**, *15*, 1894. https://doi.org/10.3390/rs15071894

Academic Editors: Massimo Menenti, Yaoming Ma, Li Jia and Lei Zhong

Received: 31 January 2023
Revised: 25 March 2023
Accepted: 30 March 2023
Published: 31 March 2023

1. Introduction

Land–atmosphere interactions play a major role in shaping and projecting regional climates [1], and studies have identified a close relationship between the strength of such interactions and extreme meteorological events such as heat waves, droughts, and heavy precipitation [2–7]. Variations in atmospheric conditions can directly alter the soil hydrothermal status by modulating meteorological conditions, such as air temperature and precipitation, while changes in the soil temperature and moisture level can trigger changes in the surface energy distribution and water balance and, ultimately, affect atmospheric processes [8–11]. Climate warming, which is caused primarily by greenhouse gas emissions, has intensified in high-latitude and mountainous regions [12,13]; inevitably, the land–atmosphere interactions in these regions can be altered and, subsequently, exert a profound impact on energy and moisture exchanges, carbon release, agricultural activity, ecosystem diversity, engineering construction and hydrological processes [14–19].

Some variables, such as the surface net radiation, sensible heat flux, and latent heat flux and ground heat flux, can directly reflect the exchange of heat between the land and atmosphere; however, long-term series of measurements of these variables are rare and difficult to obtain, especially in high-latitude and mountainous regions [20]. In contrast, variations in air and soil temperatures, which are the result of energy and moisture partitioning at the surface, have long been observed and recorded, and the difference between these two temperatures, ΔT, is commonly used to assess land–atmosphere heat exchange regimes over long periods [10]. ΔT has been identified as having a crucial influence on climates and environments at the regional and even global level [21]. Over the past few decades, considerable research has been performed to investigate the spatiotemporal variations in ΔT, as well as the relationships of this variable with environmental factors on the regional, national and hemispheric scales, using station observations, reanalysis data or satellite remote-sensing data [9,10,22–36].

Regarded as the "Third Pole of the World", the Qinghai–Tibetan Plateau (QTP) has unique topographic and thermodynamic effects that have exerted an obvious influence on the weather and climate systems of China and East Asia and have even been shown to have global effects [20,37–41]. Over the past few decades, the QTP has experienced rapid surface air warming and humidification, leading to changes in atmospheric and hydrological cycles and profound effects on regional land–atmosphere heat exchange [42,43]. Under such circumstances, increased knowledge of the spatiotemporal variations in ΔT on the QTP can inform analyses of the regional climate, ecology and other parameters. Studies have used ground observations to investigate the relationship of soil temperature at different depths with air temperature on the QTP [44–46]. However, the results of such analyses may have been subject to low-elevation bias, because the study sites were sparsely distributed, with most being less than 4000 m above sea level due to the harsh natural environment and high cost of observation. By combining in situ observations with remote sensing data, the release of reanalysis datasets provide substantial data for large-scale studies of land–atmosphere interactions with relatively high spatial and temporal resolutions [47–49], and such datasets have been used in a series of scientific studies on the QTP [11,47–54]. Using multi-source reanalysis datasets, Wang et al. (2020) investigated spatiotemporal variations in the difference between skin (0 cm of the land surface) and air temperatures from 1979 to 2018 [11]. As ecological, hydrological and biological activities mainly occur within the near-surface soil layer, understanding the exchange of heat between the shallow soil layer and the atmosphere is crucial for understanding temperature-dependent processes in fields such as regional ecology and agriculture. However, there has been little research on ΔT between shallow soil and air on the QTP.

Following the identification of a reanalysis data product with a relatively high simulation accuracy of ΔT, this study investigated the spatiotemporal variations in ΔT between shallow soil and air over the QTP. The dataset used in this study was selected from four widely used reanalysis data products on the QTP [11,50,54,55]: the Global Land Data Assimilation System (GLDAS) Version 2.0, National Centers for Environmental Prediction (NCEP) and the Department of Energy (DOE) Reanalysis 2, the fifth-generation European Centre for Medium-Range Weather Forecasts (ECMWF) atmospheric reanalysis (ERA5) and an enhanced-resolution version of the ERA5 (ERA5-land).

2. Materials and Methods

2.1. Study Area

The QTP stretches more than 2945 km from east to west and more than 1532 km from south to north, within the approximate geographic boundaries of 25°N–40°N and 73°E–105°E (Figure 1). Known as the "Roof of the World," the QTP has an average elevation exceeding 4000 m, which has promoted the development of an alpine climate characterized by strong radiation, low temperatures and a large diurnal temperature range. The QTP has an annual mean temperature of approximately −2.5 °C and annual mean precipitation of approximately 380 mm.

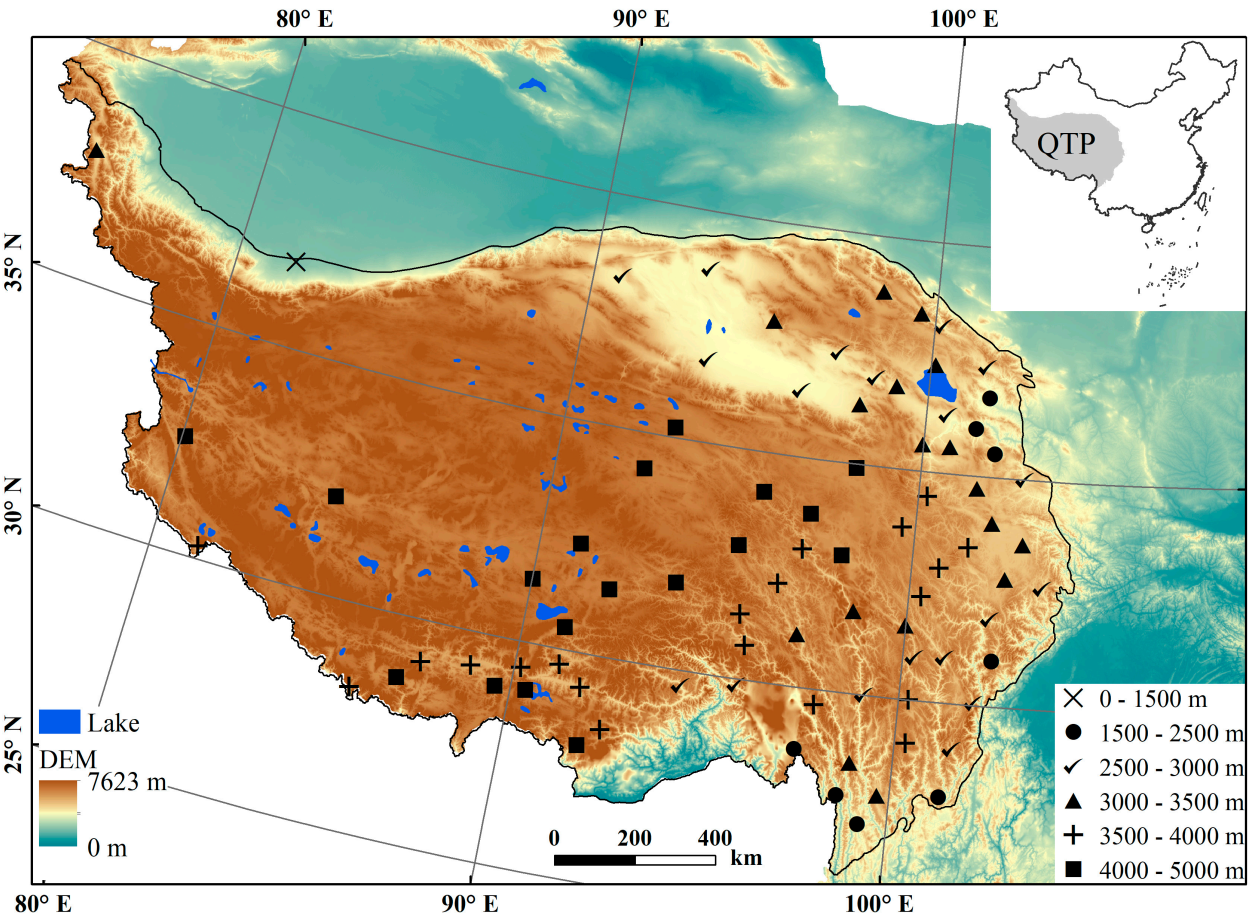

Figure 1. Location of the Qinghai–Tibetan Plateau (QTP) and the spatial distribution of 84 meteorological stations. The boundary of the QTP is provided by the National Tibetan Plateau Data Center (https://data.tpdc.ac.cn/zh-hans/data/0231c972-8460-4691-a187-70e4cc356f60 (accessed on 1 October 2022)). The background coloration reflects the altitude. DEM: digital elevation model.

2.2. Data

2.2.1. Reanalysis Data

Four reanalysis data products that contain long-term series data on soil and air temperatures were evaluated in this study (Table 1). GLDAS is a global, high-resolution, offline terrestrial modeling system that can produce optimal fields of land surface states and fluxes in near-real time [56]. GLDAS-Noah is the Noah Land Surface Model driven by GLDAS V2.0; it has a spatial resolution of 0.25° × 0.25° and provides time series from 1948 to 2015 [56,57]. NCEP-DOE Reanalysis 2 (hereafter, NCEP-R2) is an improved version of the NCEP Reanalysis 1 model; in NCEP-R2, errors have been corrected, and updated parameterizations of physical processes are provided [58] along with data at a spatial resolution of 1.875° (longitude) × 1.889° (latitude) and a time range from 1979 to the present.

Table 1. Summary of the four reanalysis datasets evaluated in this study.

Dataset	Institutes	Time Resolution (h)	Spatial Resolution	Time Period	Soil Temperature (cm)
GLDAS-Noah	NASA/NCEP	3 h	0.25° × 0.25°	1948~2015	0~10, 10~40, 40~100, 100~200
NCEP-R2	NCEP	6 h	1.875° × 1.889°	1979~present	0~10, 10~200
ERA5	ECMWF	1 h	0.25° × 0.25°	1959~present	0~7, 7~28, 28~100, 100~289
ERA5-Land	ECMWF	1 h	0.1° × 0.1°	1950~present	0~7, 7~28, 28~100, 100~289

NASA: National Aeronautics and Space Administration, USA. NCEP: National Centers for Environmental Prediction, USA. ECMWF: the European Centre for Medium-range Weather Forecasts, European.

As the fifth-generation reanalysis data product of the ECMWF, ERA5 uses data assimilation to combine model data with global observations and provides hourly values for a large number of atmospheric, ocean–wave and land–surface parameters at a spatial resolution of $0.25^\circ \times 0.25^\circ$ and a time range from 1959 to the present [59]. Compared with ERA5, ERA5-land provides a consistent view of the land variables over several decades at an enhanced resolution (i.e., $0.1^\circ \times 0.1^\circ$) from 1950 to the present and is forced by ERA5 atmospheric parameters with lapse rate correction [60–62].

2.2.2. Observational Data

In accordance with the ground meteorological observation standard of the China Meteorological Administration (CMA), meteorological stations can provide soil temperatures at depths of 0, 5, 10, 15, 20, 40, 80, 160 and 320 cm [63]. To better match the soil layer of the reanalysis products (Table 1) with the observation data, this study focused on the shallow soil layer corresponding to depths of 0~10 cm for GLDAS-Noah and NCEP-R2 products and 0~7 cm for ERA5-land and ERA5 products. A set of observed soil temperature (at depths of 0, 5 and 10 cm) collected at 84 meteorological stations within and around the QTP were used to calculate the mean shallow soil temperature at depths of 0~10 cm (Figure 1). For all 84 stations, the average elevation was 2866 m, ranging from 1422 m to 4800 m. Time series of daily air and soil temperature observations within and around the QTP were obtained from the CMA; these were measured at 02:00, 08:00, 14:00 and 20:00 Beijing time (18:00, 00:00, 06:00 and 12:00 UTC) at a height of 1.5 m above the ground and depths of 0, 5 and 10 cm, respectively. Time series of daily air temperature from the 4 reanalysis datasets corresponded to a height of 2.0 m above the ground.

2.3. Methods

We used ΔT as a metric for evaluating land–atmosphere interactions. To evaluate the performances of the four reanalysis datasets in estimating ΔT, the annual and seasonal ΔT values calculated from in situ observations within and around the QTP were compared with those calculated from the four reanalysis datasets using three evaluation indexes: the root mean square error (RMSE), mean absolute error (MAE) and mean relative error (MRE). The soil and air temperature data were extracted from the 4 products using ArcGIS software for the grid cells, corresponding to the longitude and latitude of each of the considered 84 stations.

Inevitably, the high altitude and harsh natural environment of the QTP have led to a lack of soil temperature observation data. In this study, the mean annual and seasonal soil temperatures at depths of 0, 5 and 10 cm were calculated for each station only when all monthly values were available in a year, and the values for each month were computed when daily values were available for more than three quarters of a month. The data were also divided into four seasons as follows: spring, March to May; summer, June to August; autumn, September to November; and winter, December to February of the next year. The mean shallow soil temperature was the arithmetic means of soil temperatures at depths of 0, 5 and 10 cm.

It is noteworthy that the soil temperature data provided by the ERA5-land and ERA5 products were obtained at depths of 0~7 cm, which was used to correspond with observed soil temperatures collected at depths of 0~10 cm [50]. During the baseline period (i.e., 1981–2010), the comparative analysis on the performance of the four reanalysis datasets in estimating annual and seasonal ΔT were performed. After comparison, we selected the reanalysis data product with relatively better performance in estimating ΔT and used this dataset in further in-depth investigations of the spatiotemporal variations in annual and seasonal ΔT over the QTP. Long-term trends of the variations in ΔT at the grid levels were assessed using the modified Mann–Kendall test and the Sen's slope estimator method [64,65], and the trend of ΔT across the entire QTP was estimated using a time series of anomalies (with respect to the mean ΔT from 1981 to 2010).

3. Results

3.1. Performance of the Four Reanalysis Datasets in Estimating ΔT

For the estimation of the annual ΔT, the ERA5-land and ERA5 products yielded the lowest RMSE value of 1.57 °C, followed by the GLDAS-Noah product (3.30 °C), while the NCEP-R2 product yielded the largest RMSE value of 9.62 °C. Similarly, the ERA5-land and ERA5 products yielded the smallest MAE and MRE values, whereas the NCEP-R2 product yielded the largest MAE and MRE values (Table 2).

Table 2. Error statistics of the ΔT values estimated using the 4 reanalysis data products against those calculated from the observation data of 84 stations across the QTP from 1981 to 2010.

	ERA5			ERA5-Land			GLDAS-Noah			NCEP-R2		
	RMSE	**MAE**	**MRE**	**RMSE**	**MAE**	**MRE**	**RMSE**	**MAE**	**MRE**	**RMSE**	**MAE**	**MRE**
Spring	1.85	1.76	0.39	1.94	1.86	0.41	2.29	2.22	0.49	12.31	11.61	3.27
Summer	1.33	1.22	0.25	1.32	1.22	0.24	1.74	1.64	0.30	6.30	6.16	1.51
Autumn	2.30	2.22	0.62	2.15	2.07	0.58	1.70	1.62	0.38	10.56	9.94	3.40
Winter	2.59	2.44	1.87	2.38	2.23	1.66	1.49	1.35	1.52	12.21	11.64	18.53
Annual	1.57	1.47	0.41	1.57	1.47	0.41	3.30	2.85	0.58	9.62	8.94	2.96

The ΔT values estimated using the ERA5-land and ERA5 products represent the difference between the soil temperature at depths of 0~7 cm and the air temperature at a height of 2 m above the ground. The ΔT values estimated using the GLDAS-Noah and NCEP-R2 products represent the difference between the soil temperature at depths of 0~10 cm and the air temperature at a height of 2 m.

For the estimation of the seasonal ΔT, the ERA5-land and ERA5 products performed best in spring and summer ΔT, with slight differences in the RMSE, MAE and MRE. For the autumn and winter ΔT, the GLDAS-Noah product yielded the smallest RMSE, MAE and MRE values, followed by the ERA5-land product, while NCEP-R2 product yielded the largest RMSE, MAE and MRE.

Overall, the ERA5-land and ERA5 products were superior to the other products in terms of estimating the annual, spring and summer ΔT. The GLDAS-Noah product performed best in terms of estimating the autumn and winter ΔT, followed by the ERA5-land product. Given the high spatial and time resolution of the ERA5-land product (Table 1), the ERA5-land reanalysis data product was selected for further investigation of the detailed spatiotemporal variations in the annual and seasonal ΔT over the QTP.

3.2. Spatial Distribution of ΔT

The annual and seasonal spatial distributions of the mean ΔT varied widely over the QTP during the 30-year baseline period (1981–2010) (Figure 2). The mean annual ΔT across the QTP was 4.13 °C, with a range from −8.08 °C to 11.15 °C. Positive values indicated a relatively high annual shallow soil temperature compared with the corresponding air temperature. Areas with positive ΔT values accounted for the majority of the QTP, whereas areas with negative values were found only in the southeastern and southern margins of the QTP. The areas with a mean annual ΔT exceeding 6 °C were mainly concentrated in the southeastern QTP, whereas the areas with a mean annual ΔT of 0–3 °C were mainly concentrated in the northern edge of the plateau and around the Qaidam Basin, with sporadic distribution in the western QTP.

The mean ΔT of the entire QTP was largest in winter (5.66 °C), followed by autumn (4.46 °C) and spring (3.25 °C), and smallest in summer (3.13 °C). Compared with the other three seasons, the total area with a negative value of ΔT was larger in spring and distributed mainly along the edge of the QTP, especially in the northwestern and southeastern margins. The eastern part of the plateau had a low mean ΔT in summer, which increased gradually in autumn and reached a maximum in winter (Figure 2).

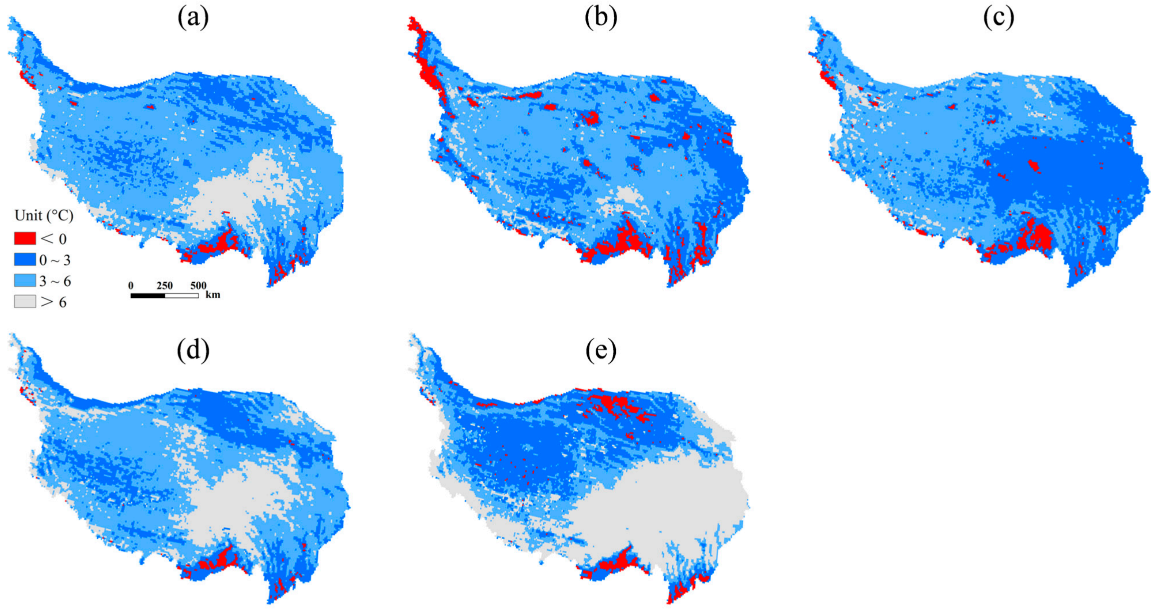

Figure 2. Geographic distribution of the mean ΔT on the QTP during the baseline period (i.e., 1981–2010); annual (**a**), spring (**b**), summer (**c**), autumn (**d**) and winter (**e**).

3.3. Changes in ΔT

Across the QTP, a significant decreasing trend in anomalies of the annual ΔT ($p < 0.01$) was observed from 1950 to 2021 at a rate of -0.07 °C/decade (Figure 3). Similarly, significant decreasing trends in ΔT ($p < 0.01$) were detected seasonally, with the largest rate of decrease in winter (-0.14 °C/decade), followed by those in autumn (-0.11 °C/decade) and summer (-0.03 °C/decade). Notably, the spring ΔT exhibited a nonsignificant increasing trend ($p = 0.43$) but no evident decreasing trend.

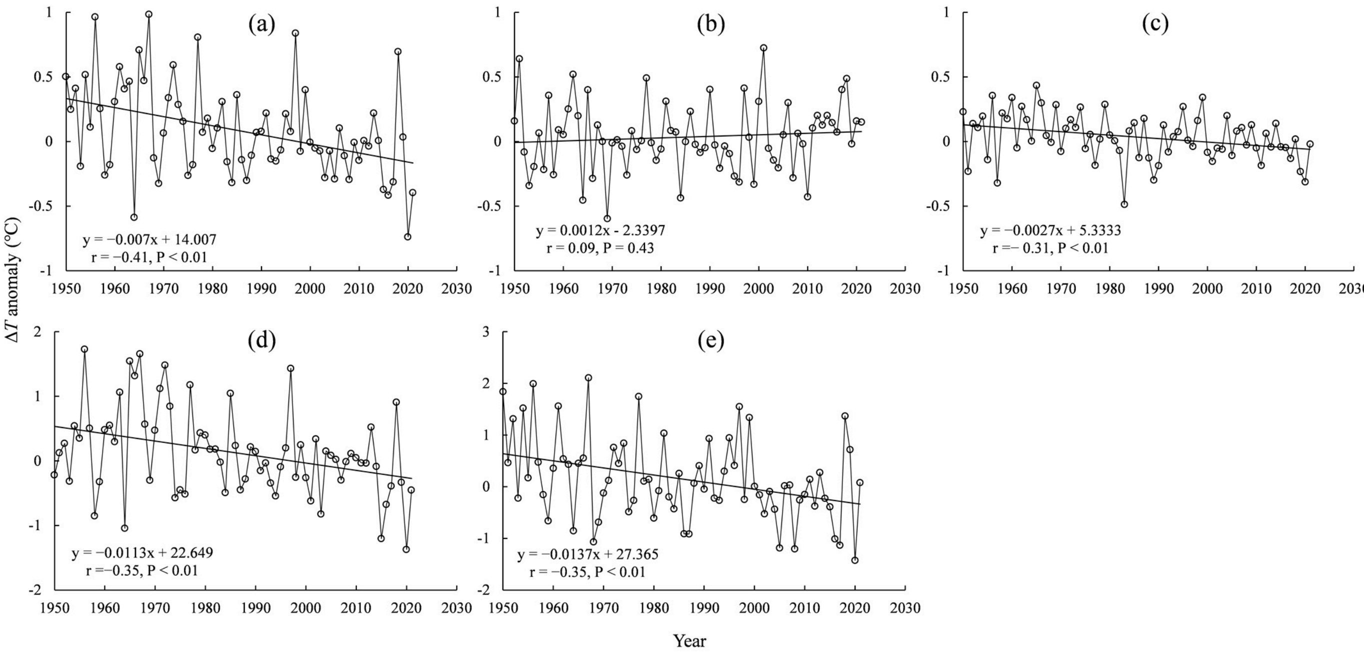

Figure 3. Changes in the mean ΔT on the QTP based on a time series of anomalies (with respect to the mean of the 30-year baseline period, i.e., 1981–2010) from 1950 to 2021; annual (**a**), spring (**b**), summer (**c**), autumn (**d**) and winter (**e**).

Compared with the mean ΔT from 1950 to 1985, the mean annual and autumn ΔT from 1986 to 2021 has decreased widely across the QTP (Figure 4). The areas with increased ΔT exceeded 50% of the entire QTP in spring, but less than 30% in summer. In winter, the magnitude of the decrease in ΔT (<−1 °C) was large in the southeastern part of the plateau. From 1950 to 2021, a large area with decreasing trends in the annual ΔT was detected, with the largest rates of decrease (e.g., −0.2 to −0.1 °C/decade, and −0.3 to −0.2 °C/decade) mainly concentrated in the southern and northeastern parts of the QTP. Spatial trends in ΔT were observed by season, with most areas showing an increasing trend in spring, especially in the central and northern parts of the plateau. During summer, autumn and winter, the proportion of the QTP with a decreasing trend in ΔT was larger than the proportion with an increasing trend. From summer, through autumn, to winter, the area with a significant decreasing trend in ΔT gradually increased in size. The largest decrease in ΔT was detected in winter, when the decreased rate of ΔT was more than 0.3 °C/decade in the southeastern part of the QTP (Figure 5).

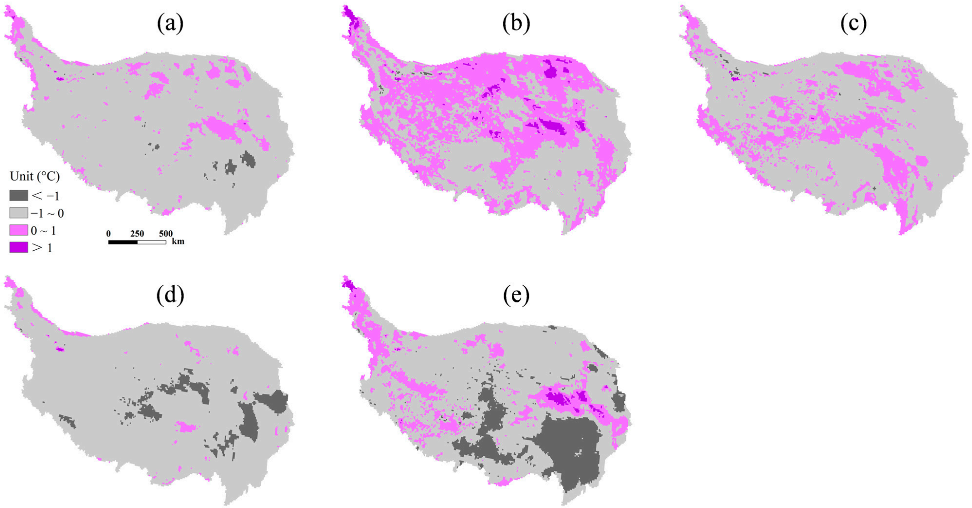

Figure 4. Spatial distributions of the difference in mean ΔT between 1986–2021 and 1950–1985 on the QTP; annual (**a**), spring (**b**), summer (**c**), autumn (**d**) and winter (**e**).

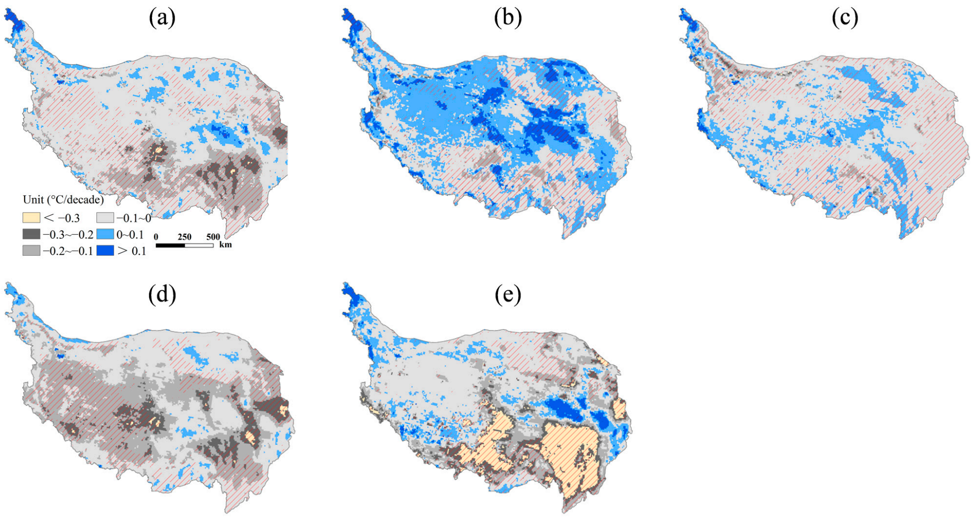

Figure 5. Geographic distribution of the rates of change in ΔT annually (**a**) and in spring (**b**), summer (**c**), autumn (**d**) and winter (**e**) on the QTP from 1950 to 2021. The oblique lines indicate significant changes in the trends at the 95% confidence level.

4. Discussion

Employing a simple metric, Δ*T*, this study aimed to assess the land–atmosphere heat exchange regime over the QTP using reanalysis data products. Similar studies have been conducted to investigate spatiotemporal variations in Δ*T* at the regional, national and hemispheric scales over the past few decades [9,10,22–36]. As ecological, hydrological and biological activities mainly occur in the near-surface soil layer, this study focused on the annual and seasonal spatiotemporal variations in Δ*T* between the shallow soil and air over the QTP.

From 1950 to 2021, both air and soil temperatures have exhibited warming trends on the QTP, especially in winter (Table 3). The asynchronism of air temperature and soil temperature variations could lead to the differences in the changes of the mean Δ*T* on the QTP both annually and seasonally (Figure 3). For example, a relatively large difference of increase in soil temperature and air temperature in winter could result in a relatively large decrease in winter Δ*T* during the study period (Table 3). Here, we investigated the possible influence of snow cover and soil moisture on Δ*T* during the study period, and precipitation is not considered, because it mainly affects the soil thermal state via soil moisture feedback in the warm season [22,28] and in the form of snow cover in the cold season. Results showed that snow depth was closely associated with the Δ*T* dynamics during the study period, except in summer (Table 3). Although snow only covers the ground during cold seasons, snow cover could modulate the land–atmosphere relationship, owing to its high albedo, low thermal conductivity and latent heat of phase changes [66]. Wang et al. (2017) reported a close association of Δ*T* with winter snow depth across China and also pointed out that such relationship might be complex and nonlinear [32]. Soil moisture conditions control the energy–water balance between the land surface and atmosphere, which can affect the surface albedo and heat capacity and then regulate the local net radiation flux and heat exchange between the land and atmosphere [3]. In this study, soil moisture was significantly and negatively correlated with summer Δ*T* during the study period (Table 3), which may be due to the soil moisture feedback. Relatively wet soil during summer may increase the energy consumption for evaporation and eventually cool the soil. During the soil freeze phase, relatively wet soil will have more liquid water freeze into ice compared with the soil with relatively low water content. This phase change leads to a greater release of latent heat and then slows down the cooling of the soil. This can partially explain why soil moisture was significantly and positively correlated with Δ*T* during autumn and winter, especially in winter (Table 3). In reality, snow cover and soil moisture are just two possible elements that influence the variation of Δ*T*. Some other regional variables, such as vegetation, air pollution and land albedo, could also affect the Δ*T* variation. Future research should, therefore, pay more attention to the investigations on the links of multiple environmental variables with Δ*T* variation.

Table 3. Changes in the mean shallow soil temperature and air temperature and correlation between the Δ*T* with snow depth and soil moisture across the QTP from 1950 to 2021.

	Change Rate (°C/Decade)		Correlation Coefficient	
	Soil Temperature	**Air Temperature**	**Snow Depth**	**Soil Moisture**
Spring	0.07	0.05	**0.25**	0.12
Summer	0.05	**0.08**	-	**−0.32**
Autumn	**0.08**	**0.18**	**0.84**	**0.37**
Winter	**0.14**	**0.26**	**0.86**	**0.46**
Annual	**0.09**	**0.17**	**0.61**	**0.25**

The soil temperature (0~7 cm), air temperature (2 m above ground), snow depth and soil moisture (0~7 cm) data were obtained from the ERA5-land products. Bold values indicate statistical significance of $p < 0.05$.

Great attention had been paid to investigate the potential causes of errors for the reanalysis products, and soil properties, input parameters, underlying surface (such as vegetation, snow cover), model structures and geographical conditions (such as altitude, aspect, slope) were thought to partially affect the simulation accuracy of air and soil temperatures [50,53,54,67–72]. In this study, the accuracy of the 4 tested reanalysis data products was compared with the observation data of 84 meteorological stations in terms of estimating ΔT and was supported by metrics, namely the MAE, RMSE and MRE. The distribution of these meteorological stations is very heterogeneous, with almost no stations in the central and western parts of the QTP (Figure 1), and this undoubtedly affected the accuracy of the validation of the estimated ΔT values when using the four reanalysis products. Therefore, more station observations and field survey data should be included in future studies.

In a previous study, the ERA5 product was found to yield the most accurate simulation of soil temperature at depths of 0~7 cm over the QTP among four tested reanalysis products (GLDAS-Noah, ERA5-land, the Climate Forecast System Reanalysis version 2 and the ECMWF interim reanalysis) [50]. Another study recommended the use of ERA5 and GLDAS-2.1 to represent air temperatures over the QTP [54]. As the ERA5-land product yielded better annual and seasonal ΔT values in our study, and its finer spatial resolution could provide more detailed spatial information about extreme events, we selected the ERA5-land reanalysis data product for our investigation of spatial and temporal changes in the annual and seasonal values of ΔT over the QTP. It is important to note, however, that the ERA5-land product was not superior to the GLDAS-Noah product in estimating the autumn and winter ΔT (Table 2). To obtain more reasonable estimations of the annual and seasonal ΔT on the QTP, future studies should consider including multiple, downscaled and remote sensing datasets with high spatial and temporal resolutions.

5. Conclusions

This study evaluated the performance of four widely used reanalysis data products, namely GLDAS-Noah, NCEP-R2, ERA5 and ERA5-land, in estimating ΔT over the QTP. The ERA5-land product provided superior estimations of ΔT both annually and seasonally, and its fine spatial resolution enabled it to provide more detailed spatial information on extreme events. Using the soil temperature at depths of 0~7 cm and air temperature at a height of 2 m above the ground, which were provided by the ERA5-Land reanalysis data product, the spatiotemporal variations in the annual and seasonal ΔT over the QTP were assessed in detail. Positive values of ΔT dominated the entire QTP both annually and seasonally during the baseline period (1981–2010), with negative annual values of ΔT only in the southeastern and southern margins of the QTP. The spatial distribution of the seasonal ΔT varied greatly, and a large area of the QTP had a negative value of ΔT in spring. In the eastern QTP, the mean ΔT was relatively small in summer, increased basically from spring to autumn and reached a maximum in winter. From 1950 to 2021, the QTP experienced significant decreasing trends in both annual and seasonal ΔT, except in spring when a nonsignificant increasing trend was observed. Spatially, the areas with higher rates of decrease in the annual ΔT were concentrated mainly in the southern and northeastern parts of the QTP, and the areas with a significant decreasing trend in ΔT gradually increased in size from summer, through autumn, to winter.

This study has some limitations. The heterogeneous distribution of the observation network on the QTP, with sparse coverage of some areas, may have reduced the accuracy of validation of the ΔT values estimated using the four reanalysis data products, and future studies should include additional station observations and field survey data. To obtain more accurate estimations of the annual and seasonal ΔT on the QTP, future studies should include multiple, high-resolution datasets that combine more station observations and field survey data.

Author Contributions: Conceptualization, X.W. and R.C.; methodology, X.W. and R.C.; validation, R.C.; formal analysis, X.W. and R.C.; data curation, X.W.; writing—original draft preparation, X.W.; funding acquisition, X.W. and R.C. All authors have read and agreed to the published version of the manuscript.

Funding: This work was supported by the National Natural Science Foundation of China (42171145 and 41901084), the National Key Research and Development Program of China (2019YFC1510505), Joint Research Project of Three-River Headwaters National Park, Chinese Academy of Sciences and The People's Government of Qinghai Province (LHZX-2020-11), and the CAS "Light of West China" Program.

Data Availability Statement: The ERA5-Land reanalysis dataset used in this study can be accessed online (https://cds.climate.copernicus.eu/cdsapp#!/dataset/reanalysis-era5-land?tab=overview (accessed on 10 October 2022)). The ERA5 reanalysis dataset used in this study can be accessed online (https://cds.climate.copernicus.eu/cdsapp#!/dataset/reanalysis-era5-single-levels?tab=overview (accessed on 10 October 2022)). The soil temperature and air temperature data for GLDAS Noah Land Surface Model L4 monthly 0.25 × 0.25 degree V2.0 can be accessed online (https://disc.gsfc.nasa.gov/datasets/GLDAS_NOAH025_3H_2.0/summary (accessed on 15 October 2022)). The soil temperature and air temperature data for NCEP-DOE Reanalysis 2 can be accessed online (https://psl.noaa.gov/data/gridded/data.ncep.reanalysis2.html (accessed on 19 October 2022)). The Daily Meteorological Dataset of basic meteorological elements of China National Surface Weather Stations provided by the China Meteorological Administration can be accessed online (http://data.cma.cn (accessed on 15 March 2022)).

Acknowledgments: The authors would like to thank the European Centre for Medium-range Weather Forecasts (ECMWF) (https://cds.climate.copernicus.eu/, (accessed on 10 October 2022)) for providing the ERA5-Land and ERA5 reanalysis datasets, National Aeronautics and Space Administration (NASA) and National Centers for Environmental Prediction (NCEP) (https://disc.gsfc.nasa.gov/, (accessed on 15 October 2022)) for providing the GLDAS Noah Land Surface Model L4 monthly 0.25 × 0.25 degree V2.0 dataset, NCEP (https://psl.noaa.gov/, (accessed on 19 October 2022)) for providing the NCEP-DOE Reanalysis 2 dataset, and China Meteorological Administration (http://data.cma.cn, (accessed on 15 March 2022)) for providing the Daily Meteorological Dataset of basic meteorological elements of China National Surface Weather Stations. The authors also would like to thank all team members at the Qilian Alpine Ecology and Hydrology Research Station, Northwest Institute of Eco-Environment and Resources, Chinese Academy of Sciences.

Conflicts of Interest: The authors declare no conflict of interest.

References

1. Council, N.R. *Assessment of Intraseasonal to Interannual Climate Prediction and Predictability*; The National Academies Press: Washington, DC, USA, 2010; p. 192.
2. Fischer, E.M.; Seneviratne, S.I.; Lüthi, D.; Schär, C. Contribution of land-atmosphere coupling to recent European summer heat waves. *Geophys. Res. Lett.* **2007**, *34*. [CrossRef]
3. Seneviratne, S.I.; Corti, T.; Davin, E.L.; Hirschi, M.; Jaeger, E.B.; Lehner, I.; Orlowsky, B.; Teuling, A.J. Investigating soil moisture–climate interactions in a changing climate: A review. *Earth-Sci. Rev.* **2010**, *99*, 125–161. [CrossRef]
4. Zhang, J.; Wang, W.-C.; Leung, L.R. Contribution of land-atmosphere coupling to summer climate variability over the contiguous United States. *J. Geophys. Res. Atmos.* **2008**, *113*, 11. [CrossRef]
5. Lorenz, R.; Argüeso, D.; Donat, M.G.; Pitman, A.J.; van den Hurk, B.; Berg, A.; Lawrence, D.M.; Chéruy, F.; Ducharne, A.; Hagemann, S.; et al. Influence of land-atmosphere feedbacks on temperature and precipitation extremes in the GLACE-CMIP5 ensemble. *J. Geophys. Res. Atmos.* **2016**, *121*, 607–623. [CrossRef]
6. Vogel, M.M.; Orth, R.; Cheruy, F.; Hagemann, S.; Lorenz, R.; van den Hurk, B.J.J.M.; Seneviratne, S.I. Regional amplification of projected changes in extreme temperatures strongly controlled by soil moisture-temperature feedbacks. *Geophys. Res. Lett.* **2017**, *44*, 1511–1519. [CrossRef]
7. García-García, A.; Cuesta-Valero, F.J.; Beltrami, H.; González-Rouco, F.; García-Bustamante, E.; Finnis, J. Land surface model influence on the simulated climatologies of temperature and precipitation extremes in the WRF v3.9 model over North America. *Geosci. Model Dev.* **2020**, *13*, 5345–5366. [CrossRef]
8. Koster, R.D.; Dirmeyer, P.A.; Guo, Z.; Bonan, G.; Chan, E.; Cox, P.; Gordon, C.T.; Kanae, S.; Kowalczyk, E.; Lawrence, D.; et al. Regions of strong coupling between soil moisture and precipitation. *Science* **2004**, *305*, 1138–1140. [CrossRef] [PubMed]
9. Feng, H.; Zou, B. A greening world enhances the surface-air temperature difference. *Sci. Total Environ.* **2019**, *658*, 385–394. [CrossRef] [PubMed]
10. García-García, A.; Cuesta-Valero, F.J.; Beltrami, H.; Smerdon, J.E. Characterization of air and ground temperature relationships within the CMIP5 historical and future climate simulations. *J. Geophys. Res. Atmos.* **2019**, *124*, 3903–3929. [CrossRef]
11. Wang, X.; Chen, D.; Pang, G.; Ou, T.; Yang, M.; Wang, M. A climatology of surface–air temperature difference over the Tibetan Plateau: Results from multi-source reanalyses. *Int. J. Climatol.* **2020**, *40*, 6080–6094. [CrossRef]

12. McBean, G. Arctic Climate: Past and Present (Chapter 2). In *Arctic Climate Impact Assessment*; Symon, C., Arris, L., Heal, B., Eds.; ACIA Scientific Report; Cambridge University Press: Cambridge, UK, 2005; pp. 21–60.
13. Pepin, N.; Bradley, R.S.; Diaz, H.F.; Baraer, M.; Caceres, E.B.; Forsythe, N.; Fowler, H.; Greenwood, G.; Hashmi, M.Z.; Liu, X.D.; et al. Elevation-dependent warming in mountain regions of the world. *Nat. Clim. Chang.* **2015**, *5*, 424–430. [CrossRef]
14. Nelson, F.E.; Anisimov, O.A.; Shiklomanov, N.I. Subsidence risk from thawing permafrost. *Nature* **2001**, *410*, 889–890. [CrossRef] [PubMed]
15. Walvoord, M.A.; Kurylyk, B.L. Hydrologic impacts of thawing permafrost—A review. *Vadose Zone J.* **2016**, *15*. [CrossRef]
16. Turetsky, M.R.; Abbott, B.W.; Jones, M.C.; Anthony, K.W.; Olefeldt, D.; Schuur, E.A.G.; Grosse, G.; Kuhry, P.; Hugelius, G.; Koven, C.; et al. Carbon release through abrupt permafrost thaw. *Nat. Geosci.* **2020**, *13*, 138–143. [CrossRef]
17. Ganjurjav, H.; Gao, Q.; Gornish, E.S.; Schwartz, M.W.; Liang, Y.; Cao, X.; Zhang, W.; Zhang, Y.; Li, W.; Wan, Y. Differential response of alpine steppe and alpine meadow to climate warming in the central Qinghai–Tibetan Plateau. *Agric. For. Meteorol.* **2016**, *223*, 233–240. [CrossRef]
18. Aalto, J.; Scherrer, D.; Lenoir, J.; Guisan, A.; Luoto, M. Biogeophysical controls on soil-atmosphere thermal differences: Implications on warming Arctic ecosystems. *Environ. Res. Lett.* **2018**, *13*, 074003. [CrossRef]
19. Wu, Q.; Zhang, Z.; Gao, S.; Ma, W. Thermal impacts of engineering activities and vegetation layer on permafrost in different alpine ecosystems of the Qinghai-Tibet Plateau, China. *Cryosphere* **2016**, *10*, 1695–1706. [CrossRef]
20. Ma, Y.; Yao, T.; Zhong, L.; Wang, B.; Xu, X.; Hu, Z.; Ma, W.; Sun, F.; Han, C.; Li, M.; et al. Comprehensive study of energy and water exchange over the Tibetan Plateau: A review and perspective: From GAME/Tibet and CAMP/Tibet to TORP, TPEORP, and TPEITORP. *Earth-Sci. Rev.* **2023**, *237*, 104312. [CrossRef]
21. Carruthers, D.J.; Stull, R.B. *An Introduction to Boundary Layer Meteorology*; Atmospheric Sciences Library: Dordrecht, The Netherlands; Kluwer: Alphen aan den Rijn, The Netherlands, 1988; Volume 13, p. 670.
22. Zhang, T.; Barry, R.G.; Gilichinsky, D.; Bykhovets, S.S.; Sorokovikov, V.A.; Ye, J. An amplified signal of climatic change in soil temperatures during the last century at Irkutsk, Russia. *Clim. Chang.* **2001**, *49*, 41–76. [CrossRef]
23. Beltrami, H.; Kellman, L. An examination of short- and long-term air–ground temperature coupling. *Glob. Planet. Chang.* **2003**, *38*, 291–303. [CrossRef]
24. Isard, S.A.; Schaetzl, R.J.; Andresen, J.A. Soils cool as climate warms in the Great Lakes region: 1951–2000. *Ann. Assoc. Am. Geogr.* **2007**, *97*, 467–476. [CrossRef]
25. Romanovsky, V.E.; Sazonova, T.S.; Balobaev, V.T.; Shender, N.I.; Sergueev, D.O. Past and recent changes in air and permafrost temperatures in eastern Siberia. *Glob. Planet. Chang.* **2007**, *56*, 399–413. [CrossRef]
26. Woodbury, A.D.; Bhuiyan, A.K.M.H.; Hanesiak, J.; Akinremi, O.O. Observations of northern latitude ground-surface and surface-air temperatures. *Geophys. Res. Lett.* **2009**, *36*. [CrossRef]
27. Lawrence, D.M.; Slater, A.G. The contribution of snow condition trends to future ground climate. *Clim. Dyn.* **2010**, *34*, 969–981. [CrossRef]
28. Qian, B.; Gregorich, E.G.; Gameda, S.; Hopkins, D.W.; Wang, X.L. Observed soil temperature trends associated with climate change in Canada. *J. Geophys. Res. Atmos.* **2011**, *116*. [CrossRef]
29. Park, H.; Sherstiukov, A.B.; Fedorov, A.N.; Polyakov, I.V.; Walsh, J.E. An observation-based assessment of the influences of air temperature and snow depth on soil temperature in Russia. *Environ. Res. Lett.* **2014**, *9*, 064026. [CrossRef]
30. Streletskiy, D.A.; Sherstiukov, A.B.; Frauenfeld, O.W.; Nelson, F.E. Changes in the 1963–2013 shallow ground thermal regime in Russian permafrost regions. *Environ. Res. Lett.* **2015**, *10*, 125005. [CrossRef]
31. Wang, W.; Rinke, A.; Moore, J.C.; Ji, D.; Cui, X.; Peng, S.; Lawrence, D.M.; McGuire, A.D.; Burke, E.J.; Chen, X.; et al. Evaluation of air–soil temperature relationships simulated by land surface models during winter across the permafrost region. *Cryosphere* **2016**, *10*, 1721–1737. [CrossRef]
32. Wang, Y.; Hu, Z.-Z.; Yan, F. Spatiotemporal variations of differences between surface air and ground temperatures in China. *J. Geophys. Res. Atmos.* **2017**, *122*, 7990–7999. [CrossRef]
33. Luo, D.; Jin, H.; Marchenko, S.S.; Romanovsky, V.E. Difference between near-surface air, land surface and ground surface temperatures and their influences on the frozen ground on the Qinghai-Tibet Plateau. *Geoderma* **2018**, *312*, 74–85. [CrossRef]
34. Shati, F.; Prakash, S.; Norouzi, H.; Blake, R. Assessment of differences between near-surface air and soil temperatures for reliable detection of high-latitude freeze and thaw states. *Cold Reg. Sci. Technol.* **2018**, *145*, 86–92. [CrossRef]
35. Zhang, Y.; Sherstiukov, A.B.; Qian, B.; Kokelj, S.V.; Lantz, T.C. Impacts of snow on soil temperature observed across the circumpolar north. *Environ. Res. Lett.* **2018**, *13*, 044012. [CrossRef]
36. Chen, L.; Aalto, J.; Luoto, M. Decadal changes in soil and atmosphere temperature differences linked with environment shifts over northern Eurasia. *J. Geophys. Res. Earth Surf.* **2021**, *126*. [CrossRef]
37. Wu, G.; Duan, A.; Liu, Y.; Mao, J.; Ren, R.; Bao, Q.; He, B.; Liu, B.; Hu, W. Tibetan Plateau climate dynamics: Recent research progress and outlook. *Natl. Sci. Rev.* **2015**, *2*, 100–116. [CrossRef]
38. Fu, Y.; Ma, Y.; Zhong, L.; Yang, Y.; Guo, X.; Wang, C.; Xu, X.; Yang, K.; Xu, X.; Liu, L.; et al. Land-surface processes and summer-cloud-precipitation characteristics in the Tibetan Plateau and their effects on downstream weather: A review and perspective. *Natl. Sci. Rev.* **2020**, *7*, 500–515. [CrossRef]
39. Duan, A.; Li, F.; Wang, M.; Wu, G. Persistent weakening trend in the spring sensible heat source over the Tibetan Plateau and its impact on the Asian summer monsoon. *J. Clim.* **2011**, *24*, 5671–5682. [CrossRef]

40. Ma, Y.M.; Hu, Z.Y.; Tian, L.D.; Zhang, F.; Yang, Y.P. Study process of the Tibet Plateau climate system change and mechanism of its impact on East Asia. *Adv. Earth Sci.* **2014**, *29*, 207–215.
41. Liu, Y.; Lu, M.; Yang, H.; Duan, A.; He, B.; Yang, S.; Wu, G. Land–atmosphere–ocean coupling associated with the Tibetan Plateau and its climate impacts. *Natl. Sci. Rev.* **2020**, *7*, 534–552. [CrossRef]
42. Yang, K.; Wu, H.; Qin, J.; Lin, C.; Tang, W.; Chen, Y. Recent climate changes over the Tibetan Plateau and their impacts on energy and water cycle: A review. *Glob. Planet. Chang.* **2014**, *112*, 79–91. [CrossRef]
43. You, Q.; Chen, D.; Wu, F.; Pepin, N.; Cai, Z.; Ahrens, B.; Jiang, Z.; Wu, Z.; Kang, S.; AghaKouchak, A. Elevation dependent warming over the Tibetan Plateau: Patterns, mechanisms and perspectives. *Earth-Sci. Rev.* **2020**, *210*, 103349. [CrossRef]
44. Fang, X.; Luo, S.; Lyu, S. Observed soil temperature trends associated with climate change in the Tibetan Plateau, 1960–2014. *Theor. Appl. Climatol.* **2019**, *135*, 169–181. [CrossRef]
45. Zhu, F.; Lan, C.; Zhang, Y.; Luo, J.J.; Lettenmaier, D.P.; Lin, Y.; Zhe, L. Spatiotemporal variations of annual shallow soil temperature on the Tibetan Plateau during 1983–2013. *Clim. Dyn.* **2018**, *51*, 2209–2227. [CrossRef]
46. Wang, X.; Chen, R.; Han, C.; Yang, Y.; Liu, J.; Liu, Z.; Guo, S.; Song, Y. Response of shallow soil temperature to climate change on the Qinghai–Tibetan Plateau. *Int. J. Climatol.* **2021**, *41*, 1–16. [CrossRef]
47. Gao, K.; Duan, A.; Chen, D.; Wu, G. Surface energy budget diagnosis reveals possible mechanism for the different warming rate among Earth's three poles in recent decades. *Sci. Bull.* **2019**, *64*, 1140–1143. [CrossRef] [PubMed]
48. Hinkelman, L.M. The global radiative energy budget in MERRA and MERRA-2: Evaluation with respect to CERES EBAF Data. *J. Clim.* **2019**, *32*, 1973–1994. [CrossRef]
49. Yang, J.; Huang, M.; Zhai, P. Performance of the CRA-40/Land, CMFD, and ERA-Interim datasets in reflecting changes in surface air temperature over the Tibetan Plateau. *J. Meteorol. Res.* **2021**, *35*, 663–672. [CrossRef]
50. Yang, S.; Li, R.; Wu, T.; Hu, G.; Xiao, Y.; Du, Y.; Zhu, X.; Ni, J.; Ma, J.; Zhang, Y.; et al. Evaluation of reanalysis soil temperature and soil moisture products in permafrost regions on the Qinghai-Tibetan Plateau. *Geoderma* **2020**, *377*, 114583. [CrossRef]
51. Qin, Y.; Zhang, P.; Liu, W.; Guo, Z.; Xue, S. The application of elevation corrected MERRA2 reanalysis ground surface temperature in a permafrost model on the Qinghai-Tibet Plateau. *Cold Reg. Sci. Technol.* **2020**, *175*, 103067. [CrossRef]
52. Xu, D.; Xin, L.A.I.; Guangzhou, F.A.N.; Jun, W.E.N.; Yuan, Y.; Xin, W.; Zuoliang, W.; Lihua, Z.H.U.; Yongli, Z.; Bingyun, W. Analysis on the applicability of reanalysis soil temperature and moisture datasets over Qinghai-Tibetan Plateau. *Plateau Meteorol.* **2018**, *37*, 626–641.
53. Hu, G.; Zhao, L.; Li, R.; Wu, X.; Wu, T.; Xie, C.; Zhu, X.; Su, Y. Variations in soil temperature from 1980 to 2015 in permafrost regions on the Qinghai-Tibetan Plateau based on observed and reanalysis products. *Geoderma* **2019**, *337*, 893–905. [CrossRef]
54. Liu, L.; Gu, H.; Xie, J.; Xu, Y.-P. How well do the ERA-Interim, ERA-5, GLDAS-2.1 and NCEP-R2 reanalysis datasets represent daily air temperature over the Tibetan Plateau? *Int. J. Climatol.* **2021**, *41*, 1484–1505. [CrossRef]
55. Zou, H.; Zhu, J.; Zhou, L.; Li, P.; Ma, S. Validation and application of reanalysis temperature data over the Tibetan Plateau. *J. Meteorol. Res.* **2014**, *28*, 139–149. [CrossRef]
56. Rodell, M.; Houser, P.R.; Jambor, U.; Gottschalck, J.; Mitchell, K.; Meng, C.J.; Arsenault, K.; Cosgrove, B.; Radakovich, J.; Bosilovich, M.; et al. The global land data assimilation system. *Bull. Am. Meteorol. Soc.* **2004**, *85*, 381–394. [CrossRef]
57. Rodell, M.; Beaudoing, H.K. *NASA/GSFC/HSL, GLDAS Noah Land Surface Model L4 Monthly 0.25 x 0.25 Degree V2.0*; Goddard Earth Sciences Data and Information Services Center (GES DISC): Greenbelt, MD, USA, 2019. [CrossRef]
58. Kanamitsu, M.; Ebisuzaki, W.; Woollen, J.; Yang, S.-K.; Hnilo, J.J.; Fiorino, M.; Potter, G.L. NCEP–DOE AMIP-II Reanalysis (R-2). *Bull. Am. Meteorol. Soc.* **2002**, *83*, 1631–1644. [CrossRef]
59. Hersbach, H.; Bell, B.; Berrisford, P.; Biavati, G.; Horányi, A.; Muñoz Sabater, J.; Nicolas, J.; Peubey, C.; Radu, R.; Rozum, I.; et al. ERA5 Hourly Data on Single Levels from 1959 to Present. Copernicus Climate Change Service (C3S) Climate Data Store (CDS). 2018. Available online: https://cds.climate.copernicus.eu/cdsapp#!/dataset/reanalysis-era5-single-levels?tab=overview (accessed on 10 October 2022).
60. Muñoz-Sabater, J.; Dutra, E.; Agustí-Panareda, A.; Albergel, C.; Arduini, G.; Balsamo, G.; Boussetta, S.; Choulga, M.; Harrigan, S.; Hersbach, H.; et al. ERA5-Land: A state-of-the-art global reanalysis dataset for land applications. *Earth Syst. Sci. Data* **2021**, *13*, 4349–4383. [CrossRef]
61. Muñoz Sabater, J. ERA5-Land Hourly Data from 1981 to Present. Copernicus Climate Change Service (C3S) Climate Data Store (CDS). 2018. Available online: https://cds.climate.copernicus.eu/cdsapp#!/dataset/reanalysis-era5-land?tab=overview (accessed on 10 October 2022).
62. Muñoz Sabater, J. ERA5-Land Hourly Data from 1950 to 1980. Copernicus Climate Change Service (C3S) Climate Data Store (CDS). 2021. Available online: https://cds.climate.copernicus.eu/cdsapp#!/dataset/reanalysis-era5-land?tab=overview (accessed on 10 October 2022).
63. China Meteorological Administration. *The Norm of Surface Meteorological Observation*; China Meteorological Press: Beijing, China, 2003; p. 151.
64. Sen, P.K. Estimates of the regression coefficient based on Kendall's Tau. *J. Am. Statal Assoc.* **1968**, *63*, 1379–1389. [CrossRef]
65. Hamed, K.H.; Rao, A.R. A modified Mann-Kendall trend test for autocorrelated data. *J. Hydrol.* **1998**, *204*, 182–196. [CrossRef]
66. Zhang, T. Influence of the seasonal snow cover on the ground thermal regime: An overview. *Rev. Geophys.* **2005**, *43*, RG4002. [CrossRef]

67. You, Q.; Kang, S.; Pepin, N.; Flügel, W.-A.; Yan, Y.; Behrawan, H.; Huang, J. Relationship between temperature trend magnitude, elevation and mean temperature in the Tibetan Plateau from homogenized surface stations and reanalysis data. *Glob. Planet. Chang.* **2010**, *71*, 124–133. [CrossRef]
68. Ding, L.; Zhou, J.; Zhang, X.; Liu, S.; Cao, R. Downscaling of surface air temperature over the Tibetan Plateau based on DEM. *Int. J. Appl. Earth Obs. Geoinf.* **2018**, *73*, 136–147. [CrossRef]
69. Hu, G.; Zhao, L.; Wu, X.; Li, R.; Wu, T.; Su, Y.; Hao, J. Evaluation of reanalysis air temperature products in permafrost regions on the Qinghai-Tibetan Plateau. *Theor. Appl. Climatol.* **2019**, *138*, 1457–1470. [CrossRef]
70. Peng, X.; Frauenfeld, O.W.; Jin, H.; Du, R.; Qiao, L.; Zhao, Y.; Mu, C.; Zhang, T. Assessment of Temperature Changes on the Tibetan Plateau During 1980–2018. *Earth Space Sci.* **2021**, *8*, e2020EA001609. [CrossRef]
71. Bi, H.; Ma, J.; Zheng, W.; Zeng, J. Comparison of soil moisture in GLDAS model simulations and in situ observations over the Tibetan Plateau. *J. Geophys. Res. Atmos.* **2016**, *121*, 2658–2678. [CrossRef]
72. Chen, Y.; Yang, K.; Qin, J.; Zhao, L.; Tang, W.; Han, M. Evaluation of AMSR-E retrievals and GLDAS simulations against observations of a soil moisture network on the central Tibetan Plateau. *J. Geophys. Res. Atmos.* **2013**, *118*, 4466–4475. [CrossRef]